

Article

# A New Family of Homoleptic Copper Complexes of Curcuminoids: Synthesis, Characterization and Biological Properties

William Meza-Morales <sup>1</sup>, Juan C. Machado-Rodríguez <sup>1</sup>, Yair Alvarez-Ricardo <sup>1</sup>,  
Marco A. Obregón-Mendoza <sup>1</sup>, Antonio Nieto-Camacho <sup>1</sup>, Rubén. A. Toscano <sup>1</sup>,  
Manuel Soriano-García <sup>1</sup>, Julia Cassani <sup>2,\*</sup> and Raúl G. Enríquez <sup>1,\*</sup>

<sup>1</sup> Instituto de Química, Universidad Nacional Autónoma de México, Circuito Exterior, Ciudad Universitaria, Mexico City C.P. 07340, Mexico; willy\_meza\_morales@hotmail.com (W.M.-M.); jcmrn.n@gmail.com (J.C.M.-R.); yfar30@hotmail.com (Y.A.-R.); obregonmendoza@yahoo.com.mx (M.A.O.-M.); camanico2015@yahoo.com (A.N.-C.); toscano@unam.mx (R.A.T.); soriano@unam.mx (M.S.-G.)

<sup>2</sup> Departamento de Sistemas Biológicos, Universidad Autónoma Metropolitana, Unidad Xochimilco, Mexico City C.P. 04960, Mexico

\* Correspondence: cassani@correo.xoc.uam.mx (J.C.); enriquezhabib@gmail.com (R.G.E.); Tel.: +52-5554837255 (J.C.); +52-5556224404 (R.G.E.); Fax: +52-5556224404 (R.G.E.)

Academic Editor: Derek J. McPhee

Received: 20 February 2019; Accepted: 2 March 2019; Published: 5 March 2019



**Abstract:** We report herein the synthesis and crystal structures of five new homoleptic copper complexes of curcuminoids. The scarcity of reports of homoleptic complex structures of curcuminoids is attributed to the lack of crystallinity of such derivatives, and therefore, their characterization by single crystal X-ray diffraction is rare. The ligand design suppressing the phenolic interaction by esterification or etherification has afforded a significant increase in the number of known crystal structures of homoleptic metal complexes of curcuminoids revealing more favorable crystallinity. The crystal structures of the present new copper complexes show four-fold coordination with a square planar geometry. Two polymorphs were found for DiBncOC-Cu when crystallized from DMF. The characterization of these new complexes was carried out using infrared radiation (IR), nuclear magnetic resonance (NMR), electron paramagnetic resonance (EPR), and single crystal X-ray diffraction (SCXRD) and the antioxidant and cytotoxic activity of the obtained complexes was evaluated.

**Keywords:** crystal structure; homoleptic copper complexes; curcuminoids; antioxidant activity

## 1. Introduction

Curcumin (1,7-bis-(4-hydroxy-3-methoxyphenyl)-1,6-heptadiene-3,5-diketone) is a metabolite of the Indian *Curcuma* species, generated by the rhizome of the perennial herb *Curcuma longa*, a member of the *gingiberacea* family widely cultivated in India and China [1]. Curcumin was isolated for the first time by Vogel and Pelletier more than two centuries ago, and Milobedzka and Lampe first proposed its chemical structure in 1910 [2,3]. Furthermore, this posed the fundamental interest that curcumin awoke gradually and expanded to other compounds that retain similar molecular topology and are denominated curcuminoids. Curcumin and curcuminoids are chelating agents due to the  $\beta$ -diketone functionality, which allow them to form stable complexes with a series of metal ions [1]. In recent years, numerous studies have been performed to better understand the medicinal properties of curcumin, curcuminoids and their metal complexes, with purported antitumor, antimicrobial, anti-inflammatory,

antioxidant, antiviral, anti-Alzheimer and anti-cancer potential [1,4–7]. Based on the wide medicinal applications reported in the literature for copper complexes, we tried to obtain copper complexes with several curcuminoids as ligands designed to promote homoleptic structures and to investigate their biological activities. However, there are very few known crystal structures of homoleptic metal complexes of curcumin and this has been attributed to an inherent low crystallinity [1,4]. In addition, they are often insoluble in water and in most common organic solvents [1]. Such property has precluded the use of single crystal X-ray diffraction as a characterization technique [1,4,8–10]. As a consequence, the studies of metal complexes of curcumin and related compounds are more focused on their biological properties [8–21] rather than in detailed structural characterizations [8–10].

In the present work, it was possible to use several curcuminoid as ligands for complexation with copper (II) i.e., acetylated curcumin (1,7-Bis (3-methoxyl-4-acetoxy) -phenol-1,6-heptadiene-3,5-diketone, DAC) **1**, hydrogenated acetylated curcumin (1,7-Bis (3-methoxyl-4-acetoxy) -phenol-heptane-3,5-diketone, DACH<sub>4</sub>) **2**, methoxylated curcumin (1,7- Bis (3,4-dimethoxy) -phenol-1,6-heptadiene-3,5-diketone, DiMeOC) **3**, benzylated curcumin (1,7-Bis (3-methoxy-4-benzyl)-phenol-1,6-heptadiene-3,5-diketone) **4**, DiBncOC and bisdemethoxy-bisdehydroxy-curcumin (1,7-diphenylhepta-1,6-diene-3,5-dione, PhCurc) **5** (see Figure 1) which proved to be suitable ligands for the formation of single crystals for X-ray studies. The characterization of all synthesized homoleptic complexes was carried out using IR, NMR and EPR in liquid state, magnetic moment, MS as well as the single crystal X-ray diffraction technique. After a full characterization was carried out, their cytotoxic and antioxidant activity was evaluated.

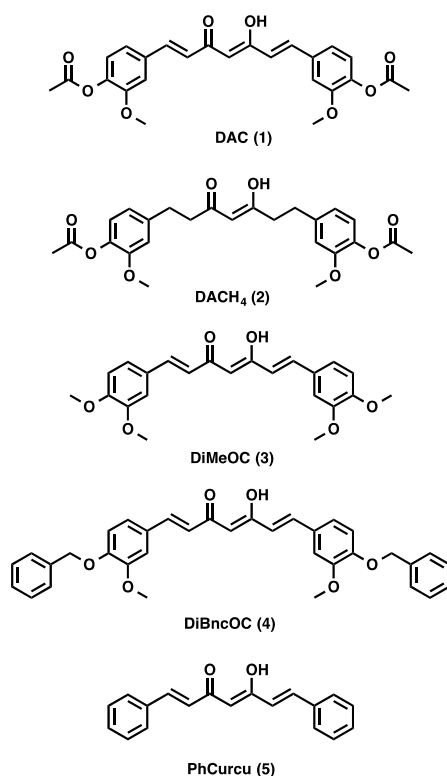


Figure 1. Ligands used for complexation with copper 1–5.

## 2. Results and Discussion

### 2.1. IR Spectra

The IR spectrum of DAC **1** shows two bands, one of high intensity at  $1755\text{ cm}^{-1}$  and another of very low intensity at  $1795\text{ cm}^{-1}$  due to the free carbonyl group of the  $\beta$ -diketone, indicating that the compound exists mainly in the enolic form. The low-intensity band in the range  $1632\text{--}1610$  is attributed to the intramolecular hydrogen bridge of the enol. The band at  $966\text{ cm}^{-1}$  that corresponds

to the trans -CH=C-double bond is also observed. The IR spectra of DAC-Cu **6** show intense bands at  $1514\text{ cm}^{-1}$  and  $\sim 484\text{ cm}^{-1}$  due to the interaction of metal  $\beta$ -diketone group from M-O vibrations. The IR spectrum of DACH<sub>4</sub> **2** shows two bands at  $1757\text{ cm}^{-1}$  (high intensity) and  $1797\text{ cm}^{-1}$  (very low intensity) showing a small ratio of the free carbonyl group of the  $\beta$ -diketone, indicating that the compound exists mainly in its enolic form (see Table 1) [13].

Three bands were observed in the range of  $2966\text{--}2841\text{ cm}^{-1}$  of low-intensity due C-H stretch. The -CH=C- band at  $965\text{ cm}^{-1}$  was not observed. IR spectra of DACH<sub>4</sub>-Cu (**7**) showed strong bands due to the interaction of the metal with the  $\beta$ -diketone group at  $1508\text{ cm}^{-1}$  and an additional band at  $\sim 467\text{ cm}^{-1}$  due to M-O vibrations. The IR spectrum of DiMeOC **3** shows the presence of two bands, one of high intensity at  $1620\text{ cm}^{-1}$  and another with very low intensity at  $1663\text{ cm}^{-1}$  due to the free carbonyl group of the  $\beta$ -diketone, revealing that the compound exists in enolic form. The trans -CH=C- band appears at  $964\text{ cm}^{-1}$ . The IR spectra of DiMeOC-Cu **8** shows strong bands due to the interaction of the metal with the  $\beta$ -diketone group at  $1506\text{ cm}^{-1}$  and an additional band at  $\sim 463\text{ cm}^{-1}$  due to M-O vibrations. The IR spectrum of DiBncOC **4** shows the presence of two bands, one of high intensity at  $1625\text{ cm}^{-1}$  and the other of very low intensity at  $1730\text{ cm}^{-1}$ , due to the free carbonyl group of the  $\beta$ -diketone. Five bands are observed in the range  $849\text{--}694\text{ cm}^{-1}$  due C-H bending. The trans -CH=C- band appears at  $970\text{ cm}^{-1}$ . IR spectra of DiBncOC-Cu **9** shows strong bands due to the interaction of the metal with the  $\beta$ -diketone group at  $1501\text{ cm}^{-1}$  and an additional band at  $\sim 465\text{ cm}^{-1}$  due to M-O vibrations. The IR spectrum of PhCurcu **5** shows the presence of two bands, one of high intensity at  $1619\text{ cm}^{-1}$  and the other of very low intensity at  $1670\text{ cm}^{-1}$ , due to the free carbonyl group of the  $\beta$ -diketone. The trans -CH=C- band appears at  $968\text{ cm}^{-1}$ . IR spectra of PhCurcu-Cu **10** show strong bands due to the interaction of the metal with the  $\beta$ -diketone group at  $1511\text{ cm}^{-1}$  and an additional band at  $\sim 420\text{ cm}^{-1}$  due to M-O vibrations (see Table 1) [13].

Table 1. IR spectral data of compounds 1–10.

Compounds	Keto-enol (cm <sup>-1</sup> )	-CH=C- (cm <sup>-1</sup> )	C-H Stretch (cm <sup>-1</sup> )	C-H Bending (cm <sup>-1</sup> )	Vibrations M-O (cm <sup>-1</sup> )
DAC	1755 and 1795	966	-	-	-
DACH <sub>4</sub>	1757 and 1797	-	2966–2841	-	-
DiMeOC	1620 and 1663	964	-	-	-
DiBcOC	1625 and 1730	970	-	849–694	-
PhCurcu	1619 and 1670	968	-	-	-
DAC-Cu	-	-	-	-	1514 and 484
DACH <sub>4</sub> -Cu	-	-	-	-	1508 and 467
DiMeOC-Cu	-	-	-	-	1506 and 463
DiBcOC-Cu	-	-	-	-	1501 and 465
PhCurcu-Cu	-	-	-	-	1511 and 420

## 2.2. NMR Spectra

The <sup>1</sup>H NMR spectrum of ligand DAC **1** shows one singlet for the OH proton at 16.12 ppm (strong intramolecular hydrogen bond) and one singlet for the methine proton at  $\sim 6.20$  ppm (vinylic proton). Protons  $\alpha$  to the diketone appear at 6.99 ppm and protons  $\beta$  to the diketone at 7.66 ppm, with a trans coupling constant of 15.9 Hz. Methoxyl and acetyl protons appear as singlets at 3.85 ppm and 2.28 ppm, respectively. The <sup>1</sup>H NMR spectrum of DACH<sub>4</sub> (ligand **2**) shows a keto-enol equilibrium with *ca.* 1:1 ratio. The enol tautomer shows one singlet for the OH proton at 15.53 ppm and one singlet for the methine proton at 5.78 ppm; both protons are involved in a strong intramolecular hydrogen bridge. The keto tautomer shows one singlet for the methylene proton at 3.74 ppm. Protons  $\alpha$  to the diketone group appear at 2.77 and 2.65 ppm while protons  $\beta$  appear at 2.85 ppm. Methoxyl and

acetyl protons appear as singlets at 3.74 ppm and 2.23 ppm, respectively. The  $^1\text{H}$  NMR spectrum of DiMeOC (ligand **3**) shows one singlet for the OH proton at 16.27 ppm and one singlet for the methine proton at 5.80 ppm; both protons are involved in a strong intramolecular hydrogen bond (enol tautomer). Protons  $\alpha$  to the diketone appear at 6.47 ppm and protons  $\beta$  to the diketone at 7.58 ppm, with a trans coupling constant of ca. 15.8 Hz. Methoxyl protons are singlets at 3.91 ppm and 3.89 ppm. The  $^1\text{H}$  NMR spectrum of DiBncOC (ligand **4**) shows one singlet for the OH proton at 16.30 ppm and one singlet for the methine proton at 6.11 ppm. Unsaturated protons  $\alpha$  to the diketone group appear at 6.84 ppm and the corresponding  $\beta$  protons at 7.59 ppm, with trans coupling constant of 15.78 Hz. Methoxyl protons are singlets at 3.84 ppm. Benzyl protons are singlets at 5.14 ppm. The  $^1\text{H}$  NMR spectrum of PhCurcu (ligand **5**) shows one singlet for the OH proton at 16.11 ppm and one singlet for the methine proton at 6.21 ppm. Protons  $\alpha$  to the diketone function appear at 6.96 ppm and protons  $\beta$  at 7.67 ppm, with a trans coupling constant of 15.97 Hz. The  $^1\text{H}$  NMR spectra of complexes **6–10** lack signals for the enol proton at ca. 16 ppm, due to paramagnetic effects (see Table 2).

**Table 2.**  $^1\text{H}$  NMR Chemical shifts ( $\delta$ ) of compounds **1–10**.

Compounds	OH ( $\delta$ )	Methine ( $\delta$ )	$\alpha$ to the Diketone ( $\delta$ )	$\beta$ to the Diketone ( $\delta$ )	Methoxyl ( $\delta$ )	Acetyl ( $\delta$ )	Benzyl ( $\delta$ )	Aromatic ( $\delta$ )
DAC	16.12	6.20	6.99	7.66	3.85	2.28	-	7.16–7.52
DACH <sub>4</sub>	15.53	5.78	2.77	2.85	3.74	2.23	-	5.78–7.00
DiMeOC	16.27	5.80	6.47	7.58	3.91–3.89	-	-	6.85–7.05
DiBcOC	16.30	6.11	6.48	7.59	3.84	-	5.14	7.34–7.59
PhCurcu	16.11	6.21	6.96	7.67	-	-	-	7.73
DAC-Cu	-	-	-	-	-	2.27	3.85	-
DACH <sub>4</sub> -Cu	-	-	-	-	-	4.01	-	-
DiMeOC-Cu	-	-	-	-	-	4.01	-	-
DiBcOC-Cu	-	-	-	-	-	3.86	-	-
PhCurcu-Cu	-	-	6.91	7.66	-	-	-	-

### 2.3. EPR Spectra

The EPR spectra of ligands show diamagnetic spectra, while the EPR spectra of copper complexes of ligands **6–10** show a typical four lines pattern (see Figure 2). The  $g_{\parallel}$ ,  $g_{\perp}$ ,  $A_{\parallel}$  and  $A_{\perp}$  values were obtained directly from the EPR spectra. The  $g_{\parallel}$  and  $g_{\perp}$  values of complexes **6–10** were ca. 2.29 and 2.06, resulting from unpaired electrons in the  $d_{x^2-y^2}$  molecular orbital [13]. The values of  $g_{\parallel}$  greater than 2.3, suggest a ionic environment for the complexes. The  $A_{\parallel}$  values ca.  $160 \times 10^{-4} \text{ cm}^{-1}$  are consistent with a typical monomeric distorted square planar geometry. The quotient  $g_{\parallel}/A_{\parallel}$  provides an index of departure from the tetrahedral structure. The quotient values that fall in the range  $105\text{--}135 \text{ cm}^{-1}$  suggest a regular square planar structure, although the observed values ( $141\text{--}146 \text{ cm}^{-1}$ ) are indicative of a strong distortion from planarity (see Table 3) [13,22–24]. The magnetic moment values for Cu(II) complexes suggest that they are paramagnetic with  $\mu_{\text{effect}}$  values of ca. 2.0 B.M with one unpaired electron (see Table 3).

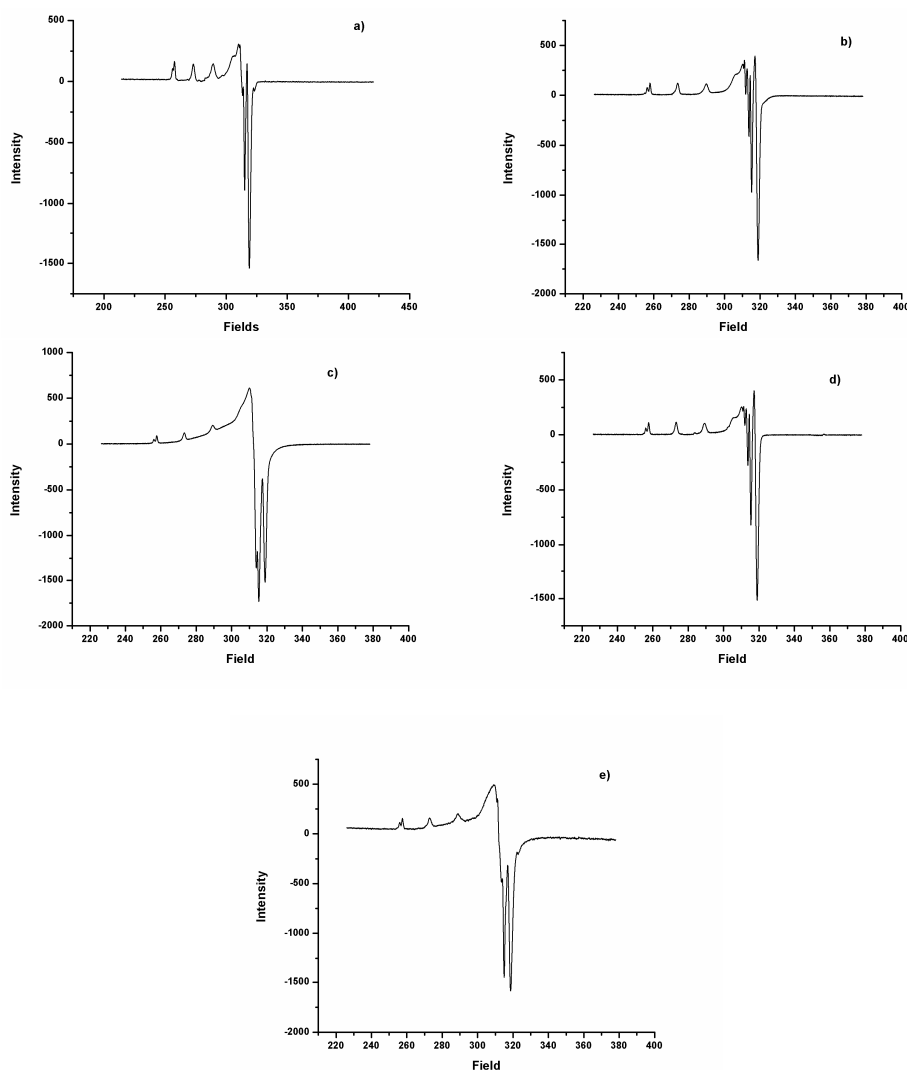


Figure 2. Spectra EPR of 6 (a), 7 (b), 8 (c) 9 (d), and 10 (e).

Table 3. EPR spectra data of copper complexes 6–10.

Complexes	$g_{\parallel}$	$g_{\perp}$	$A_{\parallel}$ ( $10^{-4}$ cm $^{-1}$ )	$A_{\perp}$ ( $10^{-4}$ cm $^{-1}$ )	$g_{\parallel}/A_{\parallel}$ (cm $^{-1}$ )	$\mu_{eff}$
DAC-Cu	2.29	2.06	162.3	11.3	141.1	1.69
DACH <sub>4</sub> -Cu	2.29	2.06	161.8	10.5	141.5	2.01
DiMeOC-Cu	2.30	2.07	160.8	9.5	143.0	1.99
DiBcOC-Cu	2.30	2.06	159.9	12.4	143.8	2.00
PhCurcu-Cu	2.30	2.07	157.3	18.11	146.3	2.09

Parallel g-value =  $g_{\parallel}$ , perpendicular g-value =  $g_{\perp}$ , parallel A-value =  $A_{\parallel}$ , perpendicular A-value =  $A_{\perp}$ .

#### 2.4. Single Crystal X-Ray Diffraction

A rigorous analysis of the crystal structure determinations of the five complexes **6**, **7**, **8**, **9a** and **10** and the triclinic polymorph **9b** (see Figure 3) reveals a four-fold coordination around copper atom with a square planar geometry (see supplementary material, Table S1), which is confirmed by the characteristics of the EPR spectra. However, if we take into consideration the “close contacts” (26.8 and 33.9% longer than the average Cu–O distances) compound, **6** and **7** can be described as 4+1 (tetragonal pyramid) and 4 + 2 (octahedron), respectively. In all compounds, the transition metal resides in a special position, except for the triclinic polymorph **9b** where the copper atom resides in a

general position. The curcuminoid ligands adopt a fully extended and almost planar conformation (see supplementary material, Table S2). It is noteworthy that these structural variations place the methyl substituents on phenols, face to face towards the inner part of the molecule in complexes 6 and 9b; all pointing outside in complex 6 and two pointing towards the inner and two pointing towards the outside in complexes 8 and 9a, revealing high conformational degrees of freedom around the (1,7-bis-(4-hydroxy-3-methoxyphenol) moiety and giving an approximately overall symmetry  $C_{2v}$  for complexes 6, 7, 9b and 10, while for complexes 8 and 9a the  $C_i$  symmetry gives the best description.

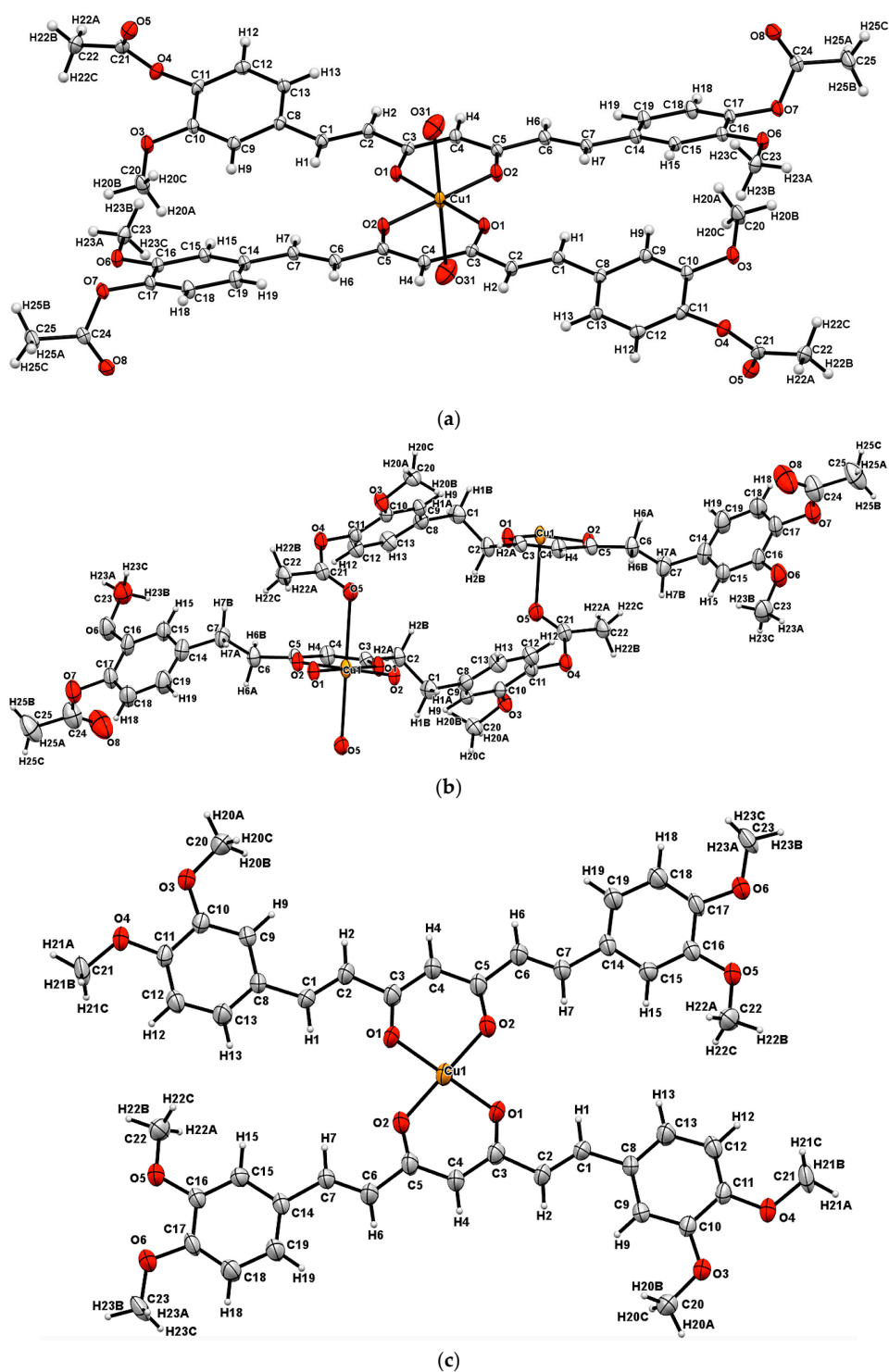
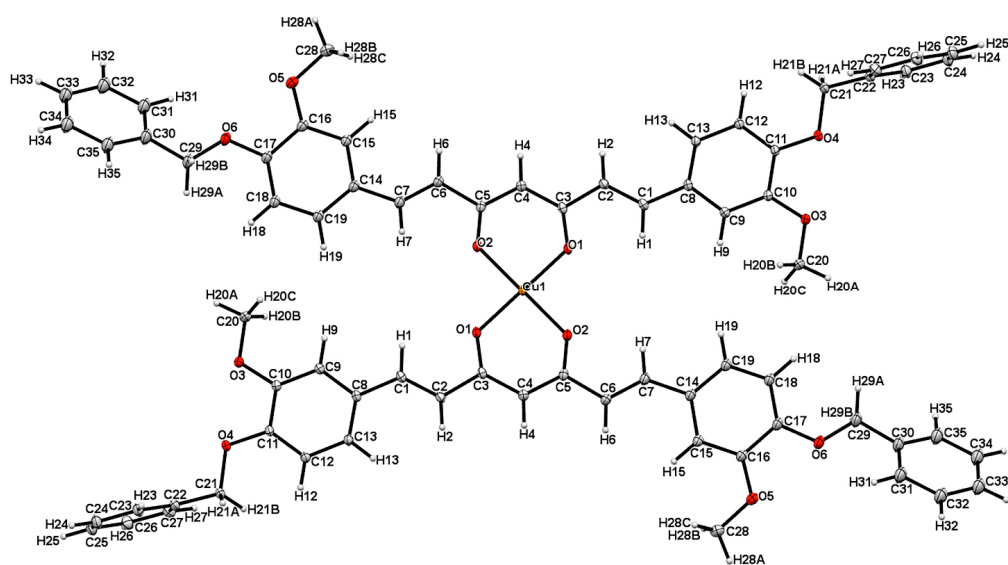
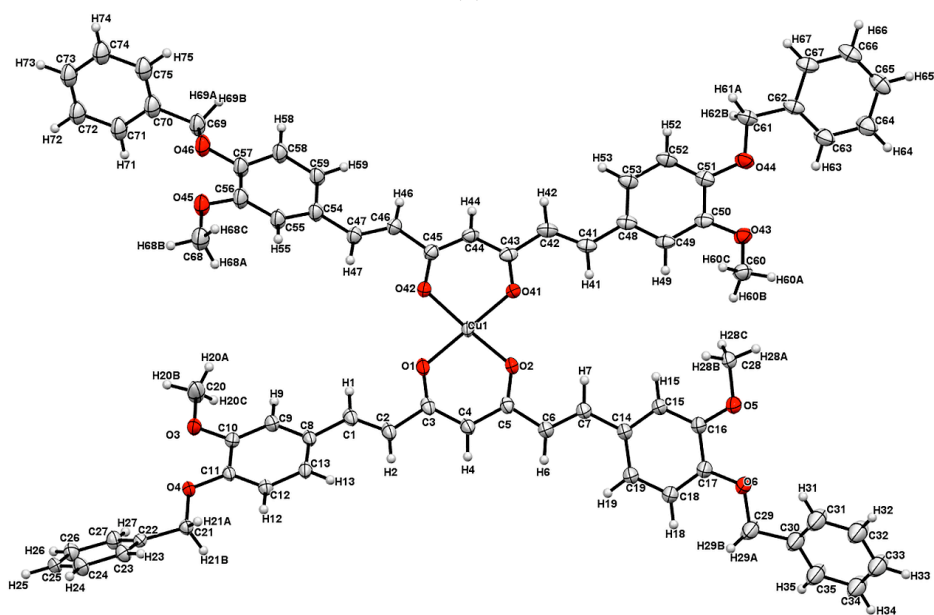


Figure 3. Cont.



(d)



(e)

Figure 3. Cont.

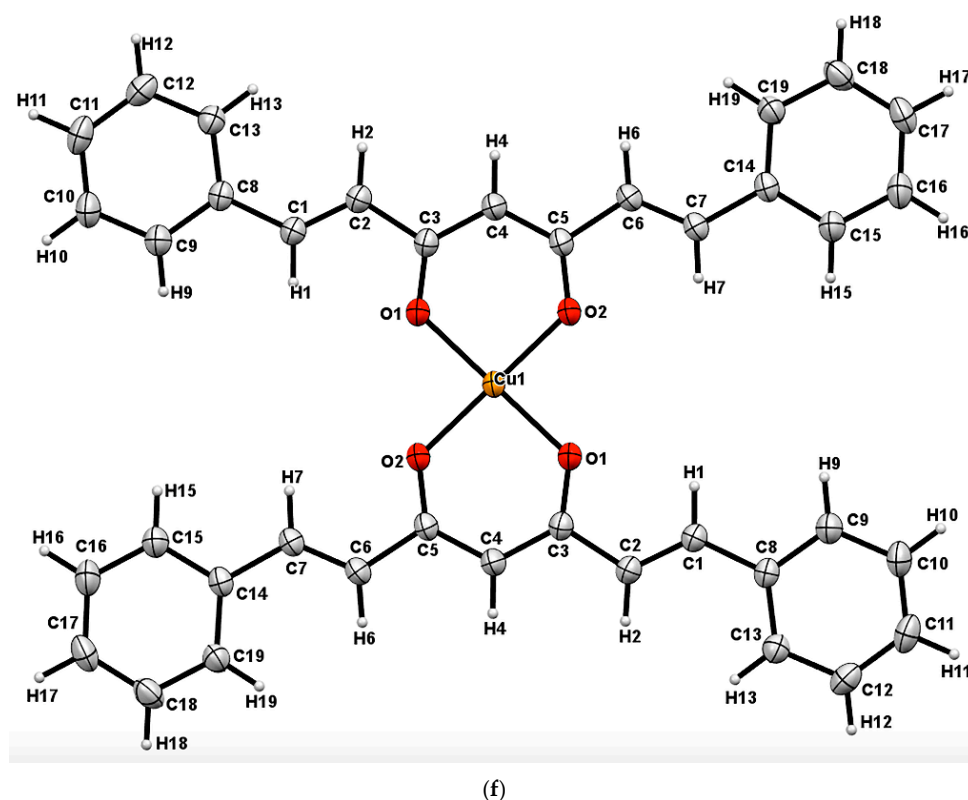


**Figure 3.** Crystal structures for **6**, **7**, **8**, **9a**, **9b** and **10** are shown in Figure 3 (a), (b), (c), (d), (e) and (f) with displacement ellipsoids at 30% probability level.

### 2.5. Inhibition of Lipoperoxidation (LP) in Rat Brain Homogenate

DAC proved to be the only ligand possessing antioxidant potential comparable to curcumin. The vinyl groups are essential for the antioxidant activity of the curcumin and curcuminoids, as it can be appreciated by the significant decrease in TBARS inhibitory percentage when going from DAC to DACH<sub>4</sub> (see Table 4). In this case, when ether groups replace the phenolic groups of curcumin, a significant decrease in the antioxidant potential is observed. Three copper complexes **6–8** showed increased antioxidant activity on the lipoperoxidation in rat brain homogenate model [25,26]. Only copper complex **9** showed a decrease in antioxidant effect respect to its ligand (see Table 4). The metal complexes **7** and **8** showed high antioxidant activity on the lipoperoxidation of rat brain homogenate model with values similar  $\alpha$ -tocopherol (see Table 5).

LP is a process initiated and mediated by reactive oxygen species (ROS), hydroxyl (HO $\cdot$ ), peroxy (ROO $\cdot$ ), alkoxy (RO $\cdot$ ) and hydroperoxy (HOO $\cdot$ ) radicals and it is known that the hydroxyl radical is an important initiator in lipid peroxidation, while peroxy and alkoxy radicals are intermediates in the propagation phase of lipid peroxidation [27]. The results shown in Table 5 suggest that the compounds exert moderate to good inhibition of ROS. The data show that Inhibitory Concentration-50 (IC<sub>50</sub>) of the free ligands DACH<sub>4</sub> and DiMeOC are ca. half as large (less active) than those observed for DACH<sub>4</sub>-Cu and DiMeOC-Cu (see Table 5), indicating that the copper complexation leads to higher activity in reducing lipid peroxidation. In general, copper is a good inducer of oxidative stress in its free form when it has the correct oxidation state. In the complexes studied in this work, copper has an oxidation state different to +1, and in our experimental conditions (pH 7.4), copper remains chelated by the ligand. Thus, the IC<sub>50</sub> values support the idea that copper remains bound to the ligands. For complexes, the IC<sub>50</sub> value is ca. half of the ligands, indicating that copper is bound to two ligand molecules. This suggests that copper is not free and does not participate as an inducer of lipid peroxidation.

**Table 4.** Lipoperoxidation Screening of ligands and their copper complexes 1–10.

Products	Concentration (uM)	D. O. 540 nm	nmol/mg prot.	Inhibition (%)
Basal	-	0.004	0.169	-
FeSO <sub>4</sub>	-	0.851	11.379	-
Curcu	10	0.000	0.116	98.67
	100	0.000	0.116	98.67
DAC	10	0.030	0.516	94.66
	100	0.012	0.275	97.16
DAC-Cu	10	0.022	0.410	95.75
	100	0.018	0.348	96.40
DACH <sub>4</sub>	10	0.313	4.257	55.95
	100	0.015	0.308	96.81
DACH <sub>4</sub> -Cu	10	0.020	0.377	96.16
	100	0.024	0.427	95.65
DiMeOC	10	0.733	9.808	1.47
	100	0.169	2.355	75.63
DiMeOC-Cu	10	0.321	4.360	55.61
	100	0.225	3.086	68.57
DiBncOC	10	0.785	10.496	7.76
	100	0.612	8.217	27.79
DiBncOC-Cu	10	0.795	10.628	6.60
	100	0.769	10.287	9.59
PhCurcu	10	0.712	9.530	8.22
	100	0.208	2.865	72.41
PhCurcu-Cu	10	0.474	6.388	38.48
	100	0.217	2.990	71.20

**Table 5.** Inhibition of lipid peroxidation IC<sub>50</sub> of compounds DAC, DACH, DiMeOC, DAC-Cu, DACH<sub>4</sub>-Cu and DiMeOC-Cu.

Products	Concentration (uM)	TBARS (nmol/mg prot.)	Inhibition (%)	IC <sub>50</sub> (uM)
Basal	-	0.24 ± 0.09	-	-
FeSO <sub>4</sub> 100 uM	-	9.15 ± 0.32	-	-
α-Tocopherol (n = 4)	0.1	6.28 ± 0.18	4.62 ± 0.57	6.78 ± 2.16
	0.32	6.04 ± 0.24	8.26 ± 1.31	
	1	5.21 ± 0.33 *	21.13 ± 2.56 *	
	3.16	3.67 ± 0.56 **	44.84 ± 6.74 **	
	10	2.72 ± 0.33 **	59.00 ± 3.71 **	
	31.62	1.84 ± 0.31 **	72.3 ± 3.87 **	
DAC	100	1.40 ± 0.36 **	79.09 ± 4.79 **	3.21 ± 0.16
	0.1	9.68 ± 0.43	4.16 ± 1.97	
	0.32	9.29 ± 0.67	8.32 ± 1.49	
	1	7.78 ± 0.53 *	23.19 ± 0.92 *	
	3.16	5.22 ± 0.35 **	48.46 ± 1.53 **	
DAC-Cu	10	1.43 ± 0.08 **	85.82 ± 0.60 **	1.55 ± 0.15
	0.1	9.08 ± 0.66	10.34 ± 1.48	
	0.32	8.04 ± 0.70	20.78 ± 2.44	
	1	6.24 ± 0.71 **	38.70 ± 3.82 **	
	3.16	3.08 ± 0.21 **	69.57 ± 1.56 **	
10	1.32 ± 0.48 **	86.58 ± 5.21 **		

Table 5. Cont.

Products	Concentration ( $\mu\text{M}$ )	TBARS (nmol/mg prot.)	Inhibition (%)	IC50 ( $\mu\text{M}$ )
DACH <sub>4</sub>	1.78	8.32 $\pm$ 0.31	9.05 $\pm$ 1.03	16.46 $\pm$ 0.30
	3.16	7.85 $\pm$ 0.41 *	14.28 $\pm$ 1.59 *	
	5.62	7.25 $\pm$ 0.36 **	20.86 $\pm$ 1.48 **	
	10	6.32 $\pm$ 0.18 **	30.84 $\pm$ 0.57 **	
	17.78	4.45 $\pm$ 0.22 **	51.41 $\pm$ 0.92 **	
	31.62	0.36 $\pm$ 0.06 **	96.02 $\pm$ 0.57 **	
	56.23	0.14 $\pm$ 0.01 **	98.39 $\pm$ 0.18 **	
DACH <sub>4</sub> -Cu	1.78	7.32 $\pm$ 0.30 **	19.93 $\pm$ 2.01 **	7.93 $\pm$ 0.41
	3.16	6.67 $\pm$ 0.34 **	27.14 $\pm$ 1.30 **	
	5.62	5.89 $\pm$ 0.33 **	35.74 $\pm$ 1.88 **	
	10	3.28 $\pm$ 0.37 **	64.27 $\pm$ 2.74 **	
	17.78	0.28 $\pm$ 0.05 **	96.90 $\pm$ 0.63 **	
	31.62	0.20 $\pm$ 0.02 **	97.73 $\pm$ 0.29 **	
	56.23	0.14 $\pm$ 0.007 **	98.39 $\pm$ 0.03 **	
DiMeOC	17.78	5.51 $\pm$ 0.13 **	38.66 $\pm$ 3.26 **	23.01 $\pm$ 1.37
	31.62	3.40 $\pm$ 0.007 **	62.16 $\pm$ 1.18 **	
	56.23	2.67 $\pm$ 0.06 **	70.33 $\pm$ 0.63 **	
	100	2.27 $\pm$ 0.09 **	74.75 $\pm$ 0.92 **	
	177.83	2.08 $\pm$ 0.10 **	76.91 $\pm$ 0.88 **	
DiMeOC-Cu	1	8.58 $\pm$ 0.28	4.55 $\pm$ 4.35	9.35 $\pm$ 0.34
	3.16	7.42 $\pm$ 0.20 **	17.51 $\pm$ 2.63 **	
	10	4.28 $\pm$ 0.06 **	52.41 $\pm$ 1.20 **	
	31.62	3.10 $\pm$ 0.12 **	65.56 $\pm$ 1.49 **	
	100	2.89 $\pm$ 0.16 **	67.90 $\pm$ 1.17 **	
	316.23	2.80 $\pm$ 0.23 **	68.97 $\pm$ 1.99 **	

Data presented as mean  $\pm$  SEM of three replicates. \*  $p \leq 0.05$  and \*\*  $p \leq 0.05$  compared to FeSO<sub>4</sub>.

## 2.6. Cytotoxic Activity

DiMeOC is the only ligand possessing higher cytotoxicity [28] than curcumin, a noteworthy fact since the phenolic groups are blocked. A significant decrease in cytotoxic activity occurs when going from DAC to DACH<sub>4</sub>, indicating the importance of conjugated double bonds in the heptanoid fragment of curcumin or curcuminoids. In general, a significant decrease in the cytotoxic activity of the copper complexes 6–10 with respect to their free ligands is observed. Interestingly compounds 6–10 did not show significant cytotoxic effect against the cell lines tested. Although there are several reports of cytotoxic or antitumor activity of copper complexes with curcumin, this effect appears to be related to the presence of free phenolic groups (see Table 6) [11,17,29].

Table 6. Cytotoxic Screening of ligands and their copper complexes 1–10.

Products (25 $\mu\text{M}$ )	% of Inhibition					
	U251	PC-3	K562	HCT-15	MCF-7	SKLU-1
DAC	46.2	77.54	67.8	46.88	41.74	41.74
DAC-Cu	8.6	13.19	19.7	4.16	NC	NC
DACH <sub>4</sub>	22.8	26.08	39.4	31.12	7.16	7.16
DACH <sub>4</sub> -Cu	NC	31.5	15.4	3.9	3.0	11.30
DiMeOC	92.6	100	89.4	96.95	100	100
DiMeOC-Cu	31.4	100	75.8	74.5	48.4	48.02
DiBncOC	3.0	10.7	10.9	NC	1.7	6.4
DiBncOC-Cu	6.6	4.1	NC	NC	NC	7.5
PhCurcu	47.5	31.2	54.7	25.0	48.7	53.0
PhCurcu-Cu	3.5	NC	4.2	NC	NC	NC

### 3. Materials and Methods

All chemicals were available commercially, and the solvents were purified by conventional methods prior to use [30]. Curcumin was obtained from natural source by usual extractive procedures and purified by crystallization.

#### 3.1. Physical Measurements

Melting points were determined on an Electrothermal Engineering IA9100X1 melting point apparatus and are uncorrected.

#### 3.2. Spectroscopic Determinations

IR absorption spectra were recorded in the range of 4000–230  $\text{cm}^{-1}$  as KBr pellets on a BRUKER Tensor 27 spectrophotometer.  $^1\text{H}$  and  $^{13}\text{C}$  NMR spectra were recorded in dimethyl sulfoxide ( $\text{DMSO}-d_6$ ) on a Bruker Fourier 300 MHz and Varian Unity Inova 500 MHz spectrometer using TMS as internal reference. The EPR spectra were recorded in DMF at liquid nitrogen temperature (77 K) on an Electron Paramagnetic Resonance Spectrometer JEOL, JES-TE300, ITC Cryogenic System, Oxford. Magnetic moments were determined using a Johnson-Matthey magnetic susceptibility balance type msb model mk II 13094-3002, with the Gouy method at room temperature. Mass spectra were recorded in a JEOL, SX 102 A spectrometer on Bruker Microflex equipped with MALDI-Flight time. Single-crystal X-ray diffractions (SCXRD) were obtained in a Bruker diffractometer, model Smart Apex, equipped with Mo radiation ( $\lambda = 0.71073\text{\AA}$ ), CCD two-dimensional detector and low-temperature device. Data collection and data reduction were performed by APEX and SAINT-Plus programs [31]. These structures were solved by direct methods using SHELX-2013 software and refined by Full-matrix least-squares procedure on F2 using SHELX-2008 program [32].

#### 3.3. Inhibition of Lipid Peroxidation on Rat Brain

##### 3.3.1. Animals

Adult male Wistar rats (200–250 g) were provided by Instituto de Fisiología Celular, Universidad Nacional Autónoma de México (UNAM). Procedures and care of animals were conducted in conformity with the Mexican Official Norm for Animal Care and Handling NOM-062-ZOO-1999. They were maintained at  $23 \pm 2$  °C under a 12/12 h light-dark cycle with *ad libitum* access to food and water.

##### 3.3.2. Rat Brain Homogenate Preparation

Animal sacrifice was carried out avoiding unnecessary pain. Rats were sacrificed with  $\text{CO}_2$ . The cerebral tissue (whole brain), was rapidly dissected and homogenized in phosphate-buffered saline (PBS) solution (0.2 g of KCl, 0.2 g of  $\text{KH}_2\text{PO}_4$ , 8 g of NaCl, and 2.16 g of  $\text{NaHPO}_4 \cdot 7\text{H}_2\text{O}$ /L, pH adjusted to 7.4) as described elsewhere to produce a 1/10 (*w/v*) homogenate [33,34]. The homogenate was centrifuged at 800 rcf (relative centrifugal field) for 10 min. The supernatant protein content was measured using Folin and Ciocalteu's phenol reagent [35] and adjusted with PBS at 2.666 mg of protein/mL.

##### 3.3.3. Induction of Lipid Peroxidation and Thiobarbituric Acid Reactive Substances (TBARS) Quantification

As an index of lipid peroxidation, TBARS levels were measured using rat brain homogenates according to the method described by Ng and co-workers [36], with some modifications. Supernatant (375  $\mu\text{L}$ ) was added with 50  $\mu\text{L}$  of 20  $\mu\text{M}$  EDTA and 25  $\mu\text{L}$  of each sample concentration dissolved in DMSO (25  $\mu\text{L}$  of DMSO for the control group) and incubated at 37 °C for 30 min. Lipid peroxidation was started adding 50  $\mu\text{L}$  of freshly prepared 100  $\mu\text{M}$   $\text{FeSO}_4$  solution (final concentration 10  $\mu\text{M}$ ) and incubated at 37 °C

for 1h. TBARS measurements were obtained as described by Ohkawa and co-workers [37], with some modifications. 500  $\mu$ L of TBA reagent (0.5% 2-thiobarbituric acid in 0.05 N NaOH and 30% trichloroacetic acid, in 1:1 ratio) was added to each tube and the final suspension cooled on ice for 10 min, centrifuged at 13,400 rcf for 5 min and heated at 80 °C in a water bath for 30 min. After cooling at room temperature, the absorbance of 200  $\mu$ L of supernatant was measured at  $\lambda = 540$  nm in a Microplate Reader Synergy/HT BIOTEK Instrument, Inc., Winooski, VT, USA. The concentration of TBARS was calculated by interpolation on a standard curve of tetra-methoxypropane (TMP) as a precursor of MDA [37]. Results are expressed as n moles of TBARS per mg of protein. The inhibition ratio (IR [%]) was calculated using the formula  $IR = (C - E) \times 100 / C$ , where C is the control absorbance, and E is the sample absorbance. Butylated hydroxytoluene (BHT) and  $\alpha$ -tocopherol were used as positive standards. All data are presented as mean  $\pm$  standard error (SEM). Data were analyzed by one-way analysis of variance (ANOVA) followed by Dunnett's test for comparison against control. Values of  $p \leq 0.05$  (\*) and  $p \leq 0.01$  (\*\*) were considered statistically significant.

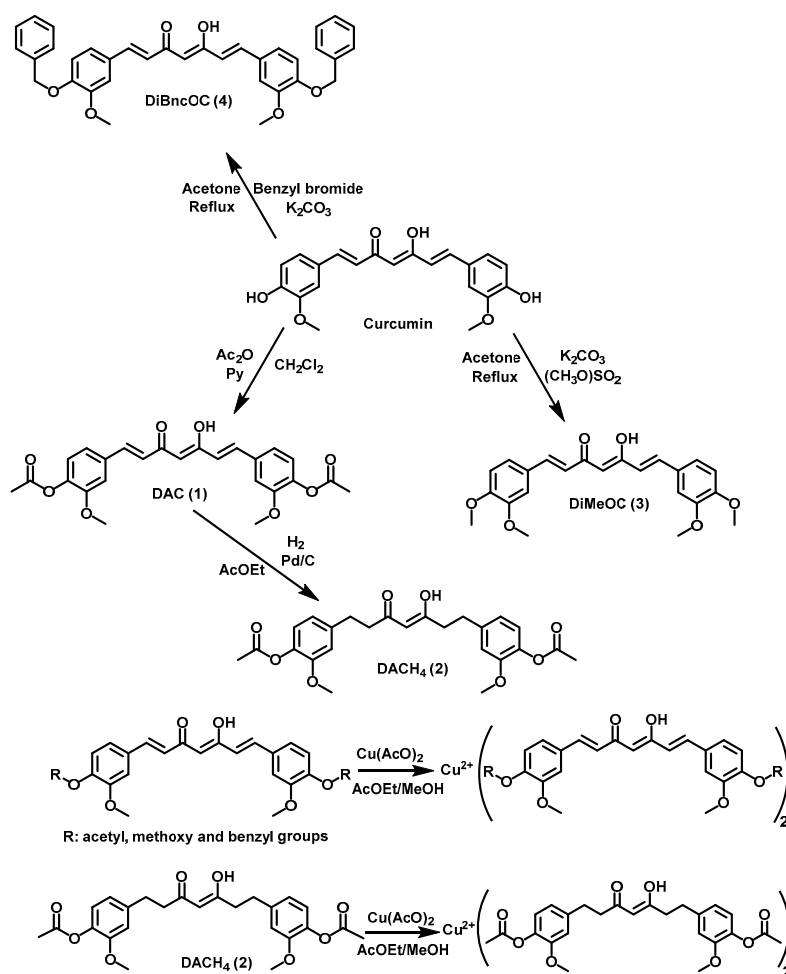
### 3.4. Cytotoxic activity in Human Tumor Cells

Cytotoxicity of all compounds was tested against six cancer cell lines: U251 (human glioblastoma cell line), PC-3 (human caucasian prostate adenocarcinoma), K562 (human caucasian chronic myelogenous leukaemia), HCT-15 (human colon adenocarcinoma), MCF-7 (human mammary adenocarcinoma) and SKLU-1 (human lung adenocarcinoma). Cell lines were supplied U.S. National Cancer Institute (NCI). The cell lines were cultured in RPMI-1640 medium supplemented with 10% fetal bovine serum, 2 mL -glutamine, 10,000 units/mL penicillin G sodium, 10,000  $\mu$ g/mL streptomycin sulfate, 25  $\mu$ g/mL amphotericin B (Invitrogen/Gibco™, Thermo Fisher Scientific, Waltham, MA, USA), and 1% non-essential amino acids (Gibco). They were maintained at 37 °C in a humidified atmosphere with 5% CO<sub>2</sub>. The viability of the cells used in the experiments exceeded 95% as determined with trypan blue. The human tumor cytotoxicity was determined using the protein-binding dye sulforhodamine B (SRB) in microculture assay to measure cell growth, as described in the protocols established by the NCI [38–40].

### 3.5. Synthesis of Compounds

General synthetic procedure for DAC **1**, DACH<sub>4</sub> **2**, DiMeOC **3**, DiBncOC **4**, DAC-Cu **6**, DACH<sub>4</sub>-Cu **7**, DiMeOC-Cu **8** and DiBncOC-Cu **9** is shown in Scheme 1.

Compound **1**. 4 g of curcumin in 70 mL of dichloromethane (CH<sub>2</sub>Cl<sub>2</sub>) was reacted with 2.6 mL of pyridine (Py) and 1.6 mL of acetic anhydride (Ac<sub>2</sub>O) at room temperature for approximately 3 h. Follow up was done by TLC. Removal of solvent from the reaction was done under reduced pressure, and the product was extracted three times with ethyl acetate (AcOEt)-water (H<sub>2</sub>O) in a 3:7 proportion of until pyridine was eliminated from the organic phase. The product recrystallized in AcOEt (**1**) with 70.1% yield. <sup>1</sup>H NMR (600 MHz DMSO-*d*<sub>6</sub>):  $\delta$  2.28 (s, 6H), 3.85 (s, 6H), 6.20 (s, 1H), 6.99 (d, 2H<sub>vinyl</sub>, J 15.9 Hz), 7.16 (d, 2H<sub>aryl</sub>, J 8.1 Hz), 7.33 (dd, 2H<sub>aryl</sub>, J 8.2; 1.9 Hz), 7.52 (d, 2H<sub>aryl</sub>, J 2 Hz), 7.66 (d, 2H<sub>vinyl</sub>, J 15.9 Hz), 16.1 (br s, 1H,) ppm, <sup>13</sup>C NMR (<sup>13</sup>C {<sup>1</sup>H} 150 MHz, DMSO-*d*<sub>6</sub>):  $\delta$  20.17 (C-H), 55.72 (C-H), 101.62 (C-H), 111.93 (C<sub>aryl</sub>), 121.27 (C<sub>aryl</sub>), 123.23 (C<sub>aryl</sub>), 124.58 (C<sub>vinyl</sub>), 133.59 (C<sub>aryl</sub>), 139.77 (C<sub>vinyl</sub>), 140.93 (C<sub>aryl</sub>), 151.11 (C<sub>aryl</sub>), 168.30 (C=O), 183.10 (C=O) ppm, IR 1755 cm<sup>-1</sup>, 1596 cm<sup>-1</sup>, 1506 cm<sup>-1</sup>, 1295 cm<sup>-1</sup>, 1154 cm<sup>-1</sup>, 619 cm<sup>-1</sup>, MS: M+ 453.15; yellow crystals, m.p. 170.5 °C.



**Scheme 1.** Synthetic route of curcuminoids and their complexes.

**Compound 2.** 3.8 g of DAC dissolved in 60 mL of AcOEt was reacted in hydrogen atmosphere with 380 mg of Pd/C-10%. The reaction mixture was stirred at room temperature until disappearance of the starting material was complete followed by TLC. The completion of reaction was achieved after 4 h and the reaction was filtered-off through celite; the solvent removed in vacuo. The product was purified by SiO<sub>2</sub> column chromatography eluting with a 7:3 hexane-AcOEt solvent mixture and the product was dried under high vacuum (2), 80.4% yield. <sup>1</sup>H NMR (500 MHz DMSO-*d*<sub>6</sub>): δ 2.23 (s, 12H), 2.65 (t, 4H<sub>aliph</sub>, J 7.86 Hz), 2.78 (m, 4H<sub>aliph</sub>), 2.85 (t, 8H<sub>aliph</sub>, J 7.02 Hz), 3.92 (d, 14H), 5.78 (s, 1H), 6.76 (dd, 2H<sub>aryl</sub>, J 8.09; 1.83 Hz), 6.79 (dd, 2H<sub>aryl</sub>, J 8.09; 1.83 Hz), 6.93 (s, 1H<sub>aryl</sub>), 6.95 (d, 2H<sub>aryl</sub>, J 2.44 Hz), 6.96 (m, 3H<sub>vinyl</sub>, Hz), 7.00 (d, 2H<sub>aryl</sub>, J 1.83 Hz), 15.51 (br s, 1H), ppm. <sup>13</sup>C NMR (<sup>13</sup>C {<sup>1</sup>H} 125 MHz, DMSO-*d*<sub>6</sub>): δ 20.17 (C-H), 29.03 (C<sub>aliph</sub>), 31.02 (C<sub>aliph</sub>), 39.44 (C<sub>aliph</sub>), 39.50 (C<sub>aliph</sub>), 44.72 (C<sub>aliph</sub>), 56.19 (C-H), 56.65 (C<sub>aliph</sub>), 100.11 (C-H), 113.25 (C<sub>aryl</sub>), 113.32 (C<sub>aryl</sub>), 120.49 (C<sub>aryl</sub>), 120.54 (C<sub>aryl</sub>), 122.90 (C<sub>aryl</sub>), 122.94 (C<sub>aryl</sub>), 137.91 (C<sub>vinyl</sub>), 138.03 (C<sub>aryl</sub>), 140.05 (C<sub>vinyl</sub>), 140.35 (C<sub>aryl</sub>), 151.02 (C<sub>aryl</sub>), 169.07 (C=O), 193.57 (C=O), 204.87 (C=O) ppm, IR 2974 cm<sup>-1</sup>, 2939 cm<sup>-1</sup>, 2841 cm<sup>-1</sup>, 1795 cm<sup>-1</sup>, 1757 cm<sup>-1</sup>, 1597 cm<sup>-1</sup>, 1510 cm<sup>-1</sup>, 1271 cm<sup>-1</sup>, 1188 cm<sup>-1</sup>, 599 cm<sup>-1</sup>, 526 cm<sup>-1</sup>, 469 cm<sup>-1</sup>, MS: M+ 455.85; white solid, m.p. 68.3 °C.

**Compound 3.** 4 g of curcumin in 120 mL of anhydrous acetone was reacted with 0.75 g of potassium carbonate (K<sub>2</sub>CO<sub>3</sub>) and 1.2 mL of dimethyl sulfate (SO<sub>2</sub>(OCH<sub>3</sub>)<sub>2</sub>) and refluxed with stirring for 48 h until disappearance of the starting material. The solvent was removed under reduced pressure and the product was extracted with a 3:7 mixture of ethyl acetate AcOEt-water (H<sub>2</sub>O) and NaOH 10% until SO<sub>2</sub>(OCH<sub>3</sub>)<sub>2</sub> was removed from the organic phase. The product was purified by SiO<sub>2</sub> column chromatography eluting with a 5:4.5:0.5 mixture of hexane-CH<sub>2</sub>Cl<sub>2</sub>-MeOH and the product

was dried under high vacuum (3), 63.2% yield. The product was recrystallized in MeOH, 65.4% yield.  $^1\text{H}$  NMR (500 MHz DMSO- $d_6$ ):  $\delta$  3.89 (s, 6H), 3.91 (s, 6H), 5.80 (s, 1H), 6.47 (d, 2H<sub>vinyl</sub>,  $J$  15.76 Hz), 6.85 (d, 2H<sub>aryl</sub>,  $J$  8.34 Hz), 7.11 (dd, 2H<sub>aryl</sub>,  $J$  8.33; 2.00 Hz), 7.05 (d, 2H<sub>aryl</sub>,  $J$  2.02 Hz), 7.58 (d, 2H<sub>vinyl</sub>,  $J$  15.80 Hz), 16.27 (br s, 1H), ppm.  $^{13}\text{C}$  NMR ( $^{13}\text{C}$  { $^1\text{H}$ } 125 MHz, DMSO- $d_6$ ):  $\delta$  60.74 (C-H), 106.16 (C-H), 115.64 (C<sub>aryl</sub>), 116.84 (C<sub>aryl</sub>), 127.20 (C<sub>aryl</sub>), 128.07 (C<sub>aryl</sub>), 132.73 (C<sub>vinyl</sub>), 145.57 (C<sub>aryl</sub>), 154.19 (C<sub>aryl</sub>), 156.14 (C<sub>aryl</sub>), 188.37 (C=O) ppm, IR 3005  $\text{cm}^{-1}$ , 2926  $\text{cm}^{-1}$ , 2831  $\text{cm}^{-1}$ , 1624  $\text{cm}^{-1}$ , 1583  $\text{cm}^{-1}$ , 1504  $\text{cm}^{-1}$ , 1134  $\text{cm}^{-1}$ , 802  $\text{cm}^{-1}$ , 607  $\text{cm}^{-1}$ , 559  $\text{cm}^{-1}$ , 544  $\text{cm}^{-1}$ , 469  $\text{cm}^{-1}$ , MS:  $M^+$  396.77; orange crystals, m.p. 133.5 °C.

Compound 4. 4 g of curcumin in 120 mL of anhydrous acetone was reacted with 0.75 g of  $\text{K}_2\text{CO}_3$  and 2.6 mL of benzyl bromide (BnBr) at reflux for approximately 30 h until the disappearance of the starting material by TLC. The reaction solvent was removed under reduce pressure. The product was purified by  $\text{SiO}_2$  column chromatography eluting with a 7:3 hexane-AcOEt solvent mixture. The product was crystallized in AcOEt, 58.7% yield.  $^1\text{H}$  NMR (500 MHz DMSO- $d_6$ ):  $\delta$  3.84 (s, 6H), 5.14 (s, 4H), 6.11 (s, H), 6.84 (d, 2H<sub>vinyl</sub>,  $J$  15.79 Hz), 7.09 (d, 2H<sub>aryl</sub>,  $J$  8.47 Hz), 7.25 (dd, 2H<sub>vinyl</sub>,  $J$  8.37; 2.00 Hz), 7.34 (t, 2H<sub>aryl</sub>,  $J$  7.22 Hz), 7.38 (d, 2H<sub>aryl</sub>,  $J$  1.94 Hz), 7.40 (t, 4H<sub>aryl</sub>,  $J$  7.36 Hz), 7.45 (dd, 4H<sub>aryl</sub>,  $J$  7.49; 2.19 Hz), 7.59 (d, 2H<sub>aryl</sub>,  $J$  15.76 Hz), 16.30 (br s, 1H).  $^{13}\text{C}$  NMR ( $^{13}\text{C}$  { $^1\text{H}$ } 125 MHz, DMSO- $d_6$ ):  $\delta$  55.65 (C-H), 69.83 (C-H), 101.06 (C-H), 110.80 (C<sub>aryl</sub>), 113.24 (C<sub>aryl</sub>), 122.18 (C<sub>aryl</sub>), 122.70 (C<sub>aryl</sub>), 127.81 (C<sub>vinyl</sub>), 128.40 (C<sub>aryl</sub>), 136.71 (C<sub>vinyl</sub>), 140.33 (C<sub>aryl</sub>), 149.30 (C<sub>aryl</sub>), 149.91 (C<sub>aryl</sub>), 183.17 (C=O) ppm, IR 3061  $\text{cm}^{-1}$ , 2922  $\text{cm}^{-1}$ , 2856  $\text{cm}^{-1}$ , 1726  $\text{cm}^{-1}$ , 1628  $\text{cm}^{-1}$ , 1585  $\text{cm}^{-1}$ , 1510  $\text{cm}^{-1}$ , 1126  $\text{cm}^{-1}$ , 970  $\text{cm}^{-1}$ , 739  $\text{cm}^{-1}$ , 696  $\text{cm}^{-1}$ , 486  $\text{cm}^{-1}$ , 459  $\text{cm}^{-1}$ , MS:  $M^+$  548.96; yellow crystals, m.p. 159.1 °C.

Compound 5. PhCurcu was prepared in accordance with a previously reported synthetic method [41], 56.7% yield.  $^1\text{H}$  NMR (500 MHz DMSO- $d_6$ ):  $\delta$  6.21 (s, 1H), 6.96 (d, 2H<sub>vinyl</sub>,  $J$  15.97 Hz), 7.45 (m, 6H), 7.67 (d, 2H<sub>vinyl</sub>,  $J$  15.92 Hz), 7.73 (dd, 4H<sub>aryl</sub>,  $J$  7.67; 1.69 Hz), 16.11 (br s, 1H) ppm, yellow crystals, m.p. 140.5 °C.

Compound 6. 1 mmol of DAC was dissolved in 30 mL of a 7:3 mixture of ethyl acetate-methanol. Then, a solution of copper acetate in MeOH and  $\text{H}_2\text{O}$  (0.5 mmol) was added dropwise. After 2 h of stirring at room temperature, a brown powder was formed, which was filtered and crystallized with DMSO, 86.9% yield.  $^1\text{H}$  NMR (500 MHz DMSO- $d_6$ ):  $\delta$  2.27 (s, 6H), 3.85 (s, 6H), 6.26 (br s, 1H), 6.81 (br s, 4H), 7.16 (br s, 1H), 7.34 (br s, 2H), 7.52 (br s, 1H), 7.66 (br s, 1H) ppm, IR 2975  $\text{cm}^{-1}$ , 2941  $\text{cm}^{-1}$ , 1752  $\text{cm}^{-1}$ , 1592  $\text{cm}^{-1}$ , 1514  $\text{cm}^{-1}$ , 1412  $\text{cm}^{-1}$ , 1299  $\text{cm}^{-1}$ , 1156  $\text{cm}^{-1}$ , 604  $\text{cm}^{-1}$ , 484  $\text{cm}^{-1}$ , brown powder, m.p. 242.5 °C.

Compound 7. 1 mmol of DACH<sub>4</sub> was dissolved in 25 mL of a 7:3 mixture of ethyl acetate-methanol and 0.5 mmol of a MeOH/ $\text{H}_2\text{O}$  solution of copper acetate was added slowly. After stirring at room temperature for 2 h, a blue powder was formed, which was filtered and crystallized in DMF/ $\text{CH}_3\text{CN}$ , 86% yield.  $^1\text{H}$  NMR (500 MHz DMSO- $d_6$ ):  $\delta$  4.01 (br s, 6H), 6.40 (br s, 2H), 7.05 (br s, 2H) ppm, IR 3020  $\text{cm}^{-1}$ , 2960  $\text{cm}^{-1}$ , 2926  $\text{cm}^{-1}$ , 2870  $\text{cm}^{-1}$ , 1759  $\text{cm}^{-1}$ , 1734  $\text{cm}^{-1}$ , 1574  $\text{cm}^{-1}$ , 1508  $\text{cm}^{-1}$ , 1196  $\text{cm}^{-1}$ , 1032  $\text{cm}^{-1}$ , 550  $\text{cm}^{-1}$ , 515  $\text{cm}^{-1}$ , 469  $\text{cm}^{-1}$ , MS:  $M^+$  973.27; blue powder, m.p. 165.8 °C.

Compound 8. 1 mmol of DiMeOC was dissolved in 30 mL of a 7:3 mixture of ethyl acetate-methanol and 0.5 mmol of a MeOH/ $\text{H}_2\text{O}$  solution of copper acetate was added dropwise. After stirring for 2 h at room temperature, a dark brown powder was formed, which was filtered and crystallized in DMSO, 93.2% yield.  $^1\text{H}$  NMR (500 MHz DMSO- $d_6$ ):  $\delta$  4.01 (br s, 6), 6.93 (br s, 5H) ppm, IR 2995  $\text{cm}^{-1}$ , 2966  $\text{cm}^{-1}$ , 2931  $\text{cm}^{-1}$ , 2843  $\text{cm}^{-1}$ , 1630  $\text{cm}^{-1}$ , 1580  $\text{cm}^{-1}$ , 1500  $\text{cm}^{-1}$ , 1421  $\text{cm}^{-1}$ , 1132  $\text{cm}^{-1}$ , 1014  $\text{cm}^{-1}$ , 968  $\text{cm}^{-1}$ , 469  $\text{cm}^{-1}$ , MS:  $M^+$  856.258; dark brown powder, m.p. 258.4 °C.

Compound 9. 1 mmol of DiBncOC was dissolved in a mixture of 50 mL tetrahydrofuran (THF), later a solution of copper acetate in MeOH and  $\text{H}_2\text{O}$  (0.5 mmol) was added slowly. After stirring at room temperature for 2 h, a brown powder was formed, which was filtered off and recrystallized from DMF, 85.7% yield.  $^1\text{H}$  NMR (500 MHz DMSO- $d_6$ ):  $\delta$  3.86 (br s, 6H), 5.01 (br s, 5H), 6.84 (br s, 6H), 7.35 (br s, 13H) ppm, IR 3030  $\text{cm}^{-1}$ , 3001  $\text{cm}^{-1}$ , 2936  $\text{cm}^{-1}$ , 1622  $\text{cm}^{-1}$ , 1502  $\text{cm}^{-1}$ , 1132  $\text{cm}^{-1}$ , 696  $\text{cm}^{-1}$ , 498  $\text{cm}^{-1}$ , 469  $\text{cm}^{-1}$ , MS:  $M^+$  1159.476; brown powder, m.p. 182.5 °C.

Compound **10**. 1 mmol of PhCurcu was dissolved in 30 mL of a 7:3 ethyl acetate-methanol mixture and 0.5 mmol of copper acetate in a MeO/H<sub>2</sub>O solution was added slowly. After stirring for 2 h at room temperature, a brown powder was formed and was filtered and crystallized in DMF, 96.3% yield. <sup>1</sup>H NMR (500 MHz DMSO-*d*<sub>6</sub>): δ 6.91 (d, 1H<sub>vinyl</sub>, *J* 15.97 Hz), 7.14 (br s, 4H), 7.45 (d, 4H<sub>aryl</sub>, *J* 5.93 Hz), 7.66 (d, 7H<sub>vinyl</sub>, *J* 19.32 Hz), IR 3023 cm<sup>-1</sup>, 1673 cm<sup>-1</sup>, 1620 cm<sup>-1</sup>, 1572 cm<sup>-1</sup>, 1070 cm<sup>-1</sup>, 641 cm<sup>-1</sup>, 590 cm<sup>-1</sup>, 510 cm<sup>-1</sup>, 420 cm<sup>-1</sup>, MS: M<sup>+</sup> 698.99; brown powder, m.p. 275.3 °C.

#### 4. Conclusions

The synthesis of 5 (compound **9** has two polymorphs) new homoleptic copper complexes was achieved with 5 different curcuminoid ligands, and their crystal structures reveal a four-fold coordination with square planar geometry. The copper ion did not increase the cytotoxic properties of the complexes with respect to free ligands but instead, high antioxidant activity for compounds DAC-Cu, DACH<sub>4</sub>-Cu and DiMeOC-Cu was found. In our results, the presence of free phenolic groups in curcumin derivatives might not be taken as the sole criterion for antioxidant or cytotoxic activity. From the pharmacological point of view, dealing with molecular species only composed by the curcuminoid and the metal atom, thus avoiding the presence of a molecular stabilizer or “spectator”, might be considered advantageous. Moreover, the synthesis of homoleptic copper complexes of curcuminoids achieved in the present work demonstrates a feasible approach for the preparation of new homoleptic complexes of curcuminoids comprising different ligands and metals.

**Supplementary Materials:** The following are available online. CCDC-1882893, CCDC-1882894, CCDC-1882895, CCDC-1882896, CCDC-1882897 and CCDC-1882898 contain the supplementary crystallographic data for this paper. These data can be obtained free of charge via [www.ccdc.cam.ac.uk/cgi-bin/catreq.cgi](http://www.ccdc.cam.ac.uk/cgi-bin/catreq.cgi), by e-mailing [data\\_request@ccdc.cam.ac.uk](mailto:data_request@ccdc.cam.ac.uk), or by contacting: The Cambridge Crystallographic Data Centre, 12 Union Road, Cambridge CB2 1EZ, UK, Fax; +44(0)-1223-336033.

**Author Contributions:** Extensive synthetic laboratory work: W.M.-M. (principal PhD student), J.C.M.-R., Y.A.-R., M.A.O.-M.; validation (X-ray extensive studies), M.S.-G., R.A.T.; Biological essays, A.N.-C.; NMR studies and funding acquisition, J.C.; writing—review and editing, project administration and funding acquisition, R.G.E. Overlapping tasks from all coauthors is thoroughly acknowledged. CRediT taxonomy.

**Funding:** We gratefully acknowledge financial support from PAPIIT (DGAPA, UNAM, IN208516) and CONACyT (CB 252524).

**Acknowledgments:** Scholarships from CONACYT awarded to WMM (No. 576707), YAR (No. 576706) and MAOM (No. 603692) are gratefully acknowledged. We are indebted to Dr. Diego Martínez Otero (X-ray), MSc. Virginia Gómez Vidales (EPR), MSc. María Teresa Ramírez Apan (cytotoxic activity) from Instituto de Química, UNAM for technical assistance, Claudia Rivera Cerecedo and Hector Malagon Rivero (biological essays) from Instituto de Fisiología Celular, UNAM. Acknowledgment is made to Dr. Rubén Gaviño (NMR), María del Rocio Patiño (IR and UV-Vis) and Lucero Rios Ruiz (EM). We gratefully acknowledge assistance from USAI (Facultad de Química, UNAM).

**Conflicts of Interest:** The authors declare no competing financial interest.

#### References

1. Wanninger, S.; Lorenz, V.; Subhan, A.; Edelmann, F.T. Metal complexes of curcumin-synthetic strategies, structures and medicinal applications. *Chem. Soc. Rev.* **2015**, *44*, 4986–5002. [[CrossRef](#)] [[PubMed](#)]
2. Ghosh, S.; Banerjee, S.; Sil, P.C. The beneficial role of curcumin on inflammation, diabetes and neurodegenerative disease: A recent update. *Food Chem. Toxicol.* **2015**, *83*, 111–124. [[CrossRef](#)] [[PubMed](#)]
3. Aggarwal, B.B.; Surh, Y.-J.; Shishodia, S. The Molecular Target and Therapeutic Uses of Curcumin in Health and Disease. In *Advances in Experimental Medicine and Biology*; Cohen, I.R., Lajtha, I.R., Lambris, J.D., Paoletti, R., Rezaei, N., Eds.; Springer: New York, NY, USA, 2007; pp. 1–75. [[CrossRef](#)]
4. Sanphui, P.; Bolla, D. Curcumin, a Biological Wonder Molecule: A Crystal Engineering Point of View. *Cryst. Growth Des.* **2018**, *9*, 5690–5711. [[CrossRef](#)]
5. Goel, A.; Kunnumakkara, A.B.; Aggarwal, B.B. Curcumin as “Curecumin”: From kitchen to clinic. *Biochem. Pharmacol.* **2008**, *75*, 787–809. [[CrossRef](#)] [[PubMed](#)]

6. Naksuriya, O.; Okonogi, S.; Schiffelers, R.M.; Hennink, W.E. Curcumin nanoformulations: A review of pharmaceutical properties and preclinical studies and clinical data related to cancer treatment. *Biomaterials* **2014**, *35*, 3365–3383. [[CrossRef](#)] [[PubMed](#)]
7. Liang, G.; Shulin, Y.; Zhou, H.; Shao, L.; Huang, K.; Xiao, J.; Huang, Z.; Li, X. Synthesis, crystal structure and anti-inflammatory properties of curcumin analogs. *Eur. J. Med. Chem.* **2009**, *44*, 915–919. [[CrossRef](#)] [[PubMed](#)]
8. Wang, J.; Wei, D.; Jiang, B.; Liu, T.; Ni, J.; Zhou, S. Two copper(II) complexes of curcumin derivatives: Synthesis, crystal structure and in vitro antitumor activity. *Transit. Met. Chem.* **2014**, *39*, 553–558. [[CrossRef](#)]
9. Aliaga-Alcalde, N.; Marqués-Gallego, P.; Kraaijkamp, M.; Herranz-Lancho, C.; Dulk, H.D.; Görner, H.; Roubeau, O.; Teat, S.J.; Weyhermüller, T.; Reedijk, J. Copper Curcuminoids Containing Anthracene Groups: Fluorescent Molecules with Cytotoxic Activity. *Inorg. Chem.* **2010**, *49*, 9655–9663. [[CrossRef](#)] [[PubMed](#)]
10. Aliaga-Alcalde, N.; Rodríguez, L.; Febinteanu, M.; Höfer, P.; Weyhermüller, T. Crystal Structure, Fluorescence, and Nanostructuring Studies of the First Zn<sup>II</sup> Anthracene-Based Curcuminoid. *Inorg. Chem.* **2012**, *51*, 864–873. [[CrossRef](#)] [[PubMed](#)]
11. Zhou, S.; Xue, X.; Jiang, B.; Tian, Y. Metal complexes of a novel bis- $\beta$ -diketone-type ligand and its copper(II) complexes of two-photon biological imaging. *Sci. China Chem.* **2012**, *55*, 334–340. [[CrossRef](#)]
12. Sarkar, T.; Butcher, R.; Banerjee, S.; Mukherjee, S.; Hussain, A. Visible light-induced cytotoxicity of a dinuclear iron(III) complex of curcumin with low-micromolar IC<sub>50</sub> value in cancer cells Dedicated to Professor Animesh Chakravorty on the occasion of his 80th birthday. *Inorg. Chim. Acta* **2016**, *439*, 8–17. [[CrossRef](#)]
13. Rajesh, J.; Gubendran, A.; Rajagopal, G.; Athappan, P. Synthesis, spectra and DNA interactions of certain mononuclear transition metal(II) complexes of macrocyclic tetra-aza diacetyl curcumin ligand. *J. Mol. Struct.* **2012**, *1010*, 169–178. [[CrossRef](#)]
14. Pi, Z.; Wang, J.; Jiang, B.; Cheng, G.; Zhou, S. A curcumin-based TPA four-branched copper(II) complex probe for in vivo early tumor detection. *Mater. Sci. Eng. C Mater. Biol. Appl.* **2015**, *46*, 565–571. [[CrossRef](#)] [[PubMed](#)]
15. Thomachan, S.; Sindhu, S.; John, V.D. Synthesis, Characterization, Antibacterial, Antifungal and Cytotoxic Activity of Curcuminoid Analogues with Trisubstituted Phenyl and Anthracenyl ring and their Zinc (II), Copper (II) and Vanadyl (IV) Chelates. *Int. J. Pharm. Chem.* **2016**, *6*, 78–86. [[CrossRef](#)]
16. Pucci, D.; Bellini, T.; Crispini, A.; D'Agnano, I.; Liguori, P.; Garcia-Orduña, P.; Pirillo, S.; Valentini, A.; Zanchetta, G. DNA binding and cytotoxicity of fluorescent curcumin-based Zn(II) complexes. *Med. Chem. Commun.* **2012**, *3*, 462–468. [[CrossRef](#)]
17. Zhang, W.; Chen, C.; Shi, H.; Yang, M.; Liu, Y.; Ji, P.; Chen, H.; Tan, R.X.; Li, E. Curcumin is a biologically active copper chelator with antitumor activity. *Phytomedicine* **2016**, *23*, 1–8. [[CrossRef](#)] [[PubMed](#)]
18. Sumanont, Y.; Murakami, Y.; Tohda, M.; Vajragupta, O.; Watanabe, H.; Matsumoto, K. Effects of Manganese Complexes of Curcumin and Diacetylcurcumin on Kainic Acid-Induced Neurotoxic Responses in the Rat Hippocampus. *Biol. Pharm. Bull.* **2007**, *30*, 1732–1739. [[CrossRef](#)] [[PubMed](#)]
19. Zhao, X.Z.; Jiang, T.; Wang, L.; Yang, H.; Zhang, S.; Zhou, P.J. Interaction of curcumin with Zn(II) and Cu(II) ions based on experiment and theoretical calculation. *J. Mol. Struct.* **2010**, *984*, 316–325. [[CrossRef](#)]
20. John, V.D.; Krishnankutty, K. Antitumour activity of synthetic curcuminoid analogs (1,7-diaryl-1,6-heptadiene-3,5-diones) and their copper complexes. *Appl. Organomet. Chem.* **2006**, *20*, 477–482. [[CrossRef](#)]
21. Asti, M.; Ferrari, E.; Croci, S.; Atti, G.; Rubagotti, S.; Iori, M.; Cappon, P.C.; Zerbini, A.; Saladini, M.; Versari, A. Synthesis and Characterization of <sup>68</sup>Ga-Labeled Curcumin and Curcuminoid Complexes as Potential Radiotracers for Imaging of Cancer and Alzheimer's Disease. *Inorg. Chem.* **2014**, *53*, 4922–4933. [[CrossRef](#)] [[PubMed](#)]
22. Attanasio, D.; Collamati, I.; Ercolani, C. Ligand arrangement in tetragonally CuO<sub>4</sub>N and CuO<sub>4</sub>N<sub>2</sub> chromophores formed from copper(II)  $\alpha$ -nitroketonates and sterically hindered N-bases. *Dalton Trans.* **1974**, 2442–2448. [[CrossRef](#)]
23. Garribba, E.; Micera, G. The Determination of the Geometry of Cu(II) Complexes an EPR Spectroscopy Experiment. *J. Chem. Educ.* **2006**, *83*, 1229–1232. [[CrossRef](#)]
24. Rajagopal, G.; Prasanna, N.; Athappan, P. Copper(II) and Ruthenium(II)/(III) Schiff base complexes. *Trans. Met. Chem.* **1999**, *24*, 251–257. [[CrossRef](#)]

25. Barik, A.; Mishra, B.; Shen, L.; Mohan, H.; Kadam, R.M.; Dutla, S.; Zhang, H.; Priyadarsini, K.L. Evaluation of a new copper(II) curcumin complex as superoxide dismutase mimic and its free radical reactions. *Free Radic. Biol. Med.* **2005**, *39*, 811–822. [[CrossRef](#)] [[PubMed](#)]
26. Banerjee, S.; Chakravarty, A.R. Metal complexes of curcumin for cellular imaging, targeting, and photoinduced anticancer activity. *Acc. Chem. Res.* **2012**, *48*, 2075–2083. [[CrossRef](#)] [[PubMed](#)]
27. Johnson, D.R.; Decker, E.A. The role of oxygen in lipid oxidation reactions: A review. *Annu. Rev. Food Sci. Technol.* **2015**, *6*, 171–194. [[CrossRef](#)] [[PubMed](#)]
28. Li, Y.; Gu, Z.; Zhang, C.; Li, S.; Zhang, L.; Zhou, G.; Wang, S.; Zhang, J. Synthesis, characterization and ROS-mediated antitumor effects of palladium(II) complexes of curcuminoids. *Eur. J. Med. Chem.* **2018**, *144*, 662–671. [[CrossRef](#)] [[PubMed](#)]
29. Wilson, J.J.; Lippard, S.J. Synthetic methods for the preparation of platinum anticancer complexes. *Chem. Rev.* **2014**, *114*, 4470–4495. [[CrossRef](#)] [[PubMed](#)]
30. Armarego, W.L.F.; Perrin, D.D. *Purification of Laboratory Chemicals*, 6th ed.; Butterworth Heinemann: Oxford, UK, 2009; pp. 138–159.
31. Bruker. *APEX2, and SAINT-Plus*; Bruker AXS Inc.: Madison, WI, USA, 2004.
32. Sheldrick, G.M. A short history of SHELX. *Acta Crystallogr. Sec. A* **2008**, *64*, 112–122. [[CrossRef](#)] [[PubMed](#)]
33. Domínguez, M.; Nieto, A.; Marín, J.C.; Keck, A.S.; Jeffery, E.; Céspedes, C.L. Antioxidant activities of extracts from *Barkleyanthus salicifolius* (Asteraceae) and *Penstemon gentianoides* (Scrophulariaceae). *J. Agric. Food Chem.* **2005**, *53*, 5889–5895. [[CrossRef](#)] [[PubMed](#)]
34. Rossato, J.I.; Ketzler, L.A.; Centuriao, F.B.; Silva, S.J.; Lüdtkke, D.S.; Zeni, G.; Braga, A.L.; Rubin, M.A.; Rocha, B.T. Antioxidant properties of new chalcogenides against lipid peroxidation in rat brain. *Neurochem. Res.* **2002**, *27*, 297–303. [[CrossRef](#)] [[PubMed](#)]
35. Lowry, O.H.; Rosebrough, N.J.; Farr, A.L.; Randall, R.J. Protein measurement with the Folin phenol reagent. *J. Biol. Chem.* **1951**, *193*, 265–275. [[PubMed](#)]
36. Ng, T.B.; Liu, F.; Wang, Z.T. Antioxidative activity of natural products from plants. *Life Sci.* **2000**, *66*, 709–723. [[CrossRef](#)]
37. Ohkawa, H.; Ohishi, N.; Yagi, K. Assay for lipid peroxides in animal tissues by thiobarbituric acid reaction. *Anal. Biochem.* **1979**, *95*, 351–358. [[CrossRef](#)]
38. Monks, A.; Scudiero, D.; Skehan, P.; Shoemaker, R.; Paul, K.; Vistica, D.; Hose, C.; Langley, J.; Cronise, P.; Vaigro-Wolff, A.; et al. Feasibility of a high-flux anticancer drug screen using a diverse panel of cultured human tumor cell lines. *J. Natl. Cancer Inst.* **1991**, *38*, 757–766. [[CrossRef](#)]
39. Sumantran, V.N. Cellular chemosensitivity assays: An overview. In *Cancer Cell Culture: Methods and Protocols*, 2nd ed.; Cree, I.A., Ed.; Humana Press: New York, NY, USA, 2011; Chapter 19; pp. 219–236.
40. Lozada, C.; Soria-Arteche, O.; Ramírez-Apan, M.T.; Nieto-Camacho, A.; Enríquez, R.G.; Izquierdo, T.; Jiménez-Corona, A. Synthesis, cytotoxic and antioxidant evaluations of amino derivatives. *Bioorg. Med. Chem.* **2012**, *20*, 5077–5084. [[CrossRef](#)] [[PubMed](#)]
41. Akram Khan, M.; El-Khatib, R.; Rainsford, K.D.; Whitehouse, M.W. Synthesis and anti-inflammatory properties of some aromatic and heterocyclic curcuminoids. *Bioorg. Chem.* **2012**, *40*, 30–38. [[CrossRef](#)] [[PubMed](#)]

**Sample Availability:** Samples of the compounds are not available from the authors.



© 2019 by the authors. Licensee MDPI, Basel, Switzerland. This article is an open access article distributed under the terms and conditions of the Creative Commons Attribution (CC BY) license (<http://creativecommons.org/licenses/by/4.0/>).